Dynamic Performance Assessment of Intelligent AGC Controllers and Multi-FACTS Devices in a Renewable-Integrated Deregulated Three-Area Power System

Mathe Ramakrishna Raju[1], Dr.N. Visali[2]
[1]*Research Scholar, Department of Electrical and Electronics Engineering, JNTUA College of Engineering, Ananthapuram, Andhra Pradesh, INDIA*
[2]*Senior Professor, Department of Electrical and Electronics Engineering, JNTUA College of Engineering, Ananthapuram, Andhra Pradesh, INDIA*

***Abstract*—This paper evaluates dynamic performance of five automatic generation control (AGC) structures and six FACTS support configurations in a renewable-integrated deregulated three-area power system. A balanced nominal design crosses 27 operating patterns, three markets, five controllers and six FACTS conditions, yielding 2,430 simulations. The system-level settling time is defined by simultaneous frequency and scheduled tie-line error recovery. Mean settling time decreases from 35.56 s for PI to 17.79 s for AI-MSFPID (50.0%), and the mean composite dynamic index decreases from 17.259 to 5.071 (70.6%). The incremental improvement from MSFPID to AI-MSFPID is substantially smaller than the improvement from conventional controllers. STATCOM and UPFC reduce mean peak frequency deviation by about 4%, while UPFC also reduces peak tie-line error by about 7.5% relative to No FACTS. Results are interpreted as comparative evidence within the specified deterministic model; they do not establish universal superiority or grid-code compliance.**

***Index Terms*—Automatic generation control; frequency deviation; tie-line power; area control error; FACTS; intelligent controller; deregulated power system.**

I. INTRODUCTION

Secondary frequency regulation must restore frequency and scheduled inter-area interchange after load or renewable-power disturbances. In a deregulated power system, these objectives are coupled to contractual transfers between distribution companies (DISCOs) and generation companies (GENCOs). An apparent change in tie-line flow is not necessarily an AGC error: the relevant control variable is the deviation from the interchange scheduled by the contracts. This distinction is essential when PoolCo, bilateral and contract-violation transactions are compared [1], [2].

Renewable generation changes the disturbance profile confronting secondary control. Wind and solar power variations affect the instantaneous area power balance, while battery energy storage systems (BESS) and aggregated electric vehicles (EVs) can provide supplementary fast response. The technical question is not simply whether a sophisticated controller can reduce an error index, but which combination of controller and network support offers a worthwhile operational improvement under changing contractual conditions.

Controller comparisons are often framed around a single aggregate score. Such a score can conceal trade-offs: a configuration may produce a small settling time yet permit a comparatively large initial frequency excursion, or suppress tie-line peaks without improving the overall recovery index. Likewise, a flexible AC transmission system device can change the network path of an error without changing the essential closed-loop governor dynamics. An operator must therefore separate recovery, peak containment, market sensitivity and implementation complexity.

The present manuscript offers a decision-oriented interpretation of existing numerical results for a three-area renewable-integrated AGC study. The source database contains 2,430 completed simulations and was also used in a separately submitted response-surface modelling (RSM) and multi-response optimisation manuscript by the same authors. This

paper does not claim to generate a second independent dataset, propose a new controller, or re-estimate the RSM models. Its narrower emphasis is the practical meaning of controller increments, network-support trade-offs and market-specific peak behaviour. Editorial acceptance as a separate publication depends on the journals' assessment of substantive distinctness and disclosure.

Three questions organise the comparison. First, how much of the apparent advantage of an AI-assisted controller is attributable to the underlying fuzzy and multi-stage control architecture? Second, which FACTS options preferentially reduce frequency peaks or tie-line excursions, and is the effect large enough to justify a device-specific recommendation? Third, do deregulated market arrangements change the recovery mechanism, or primarily alter the magnitude of the disturbance seen by AGC?

Donde et al. [1] and Demiroren and Zeynelgil [2] established the importance of contract-aware AGC modelling. Dash et al. [3] compared FACTS-assisted multi-area control, and Pilla et al. [4] examined FACTS selection with fuzzy PID. More recent studies address renewable and EV participation in deregulated systems [5]. These contributions motivate evaluating controller and network support jointly. The distinctive value of the present analysis is not a novel algorithm; it is the explicit interpretation of the magnitude and direction of performance differences across a balanced set of existing simulated operating cases.

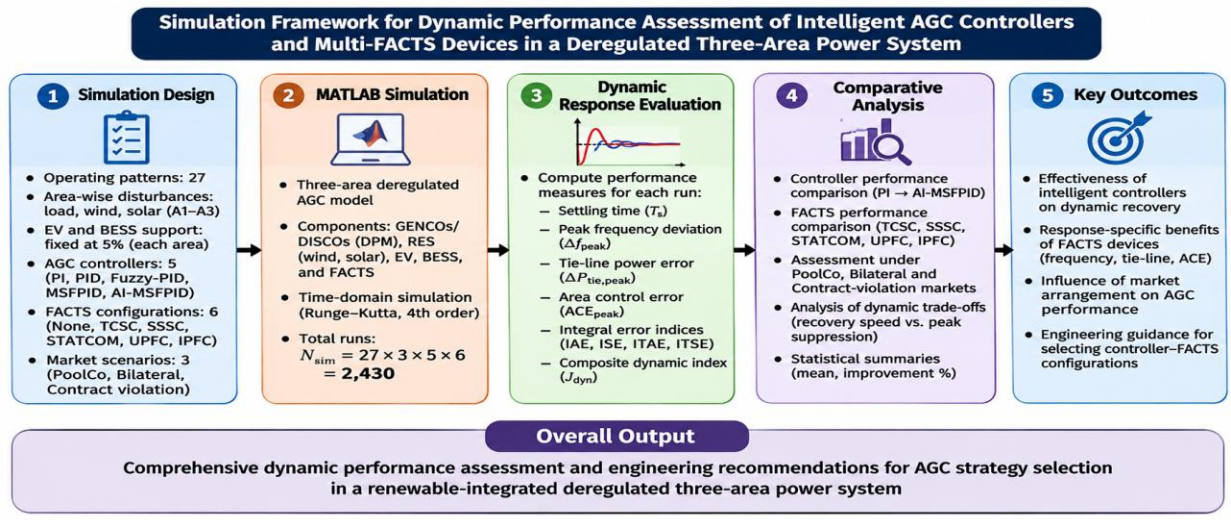


Fig. 1. Simulation framework for comparative dynamic performance assessment of intelligent AGC controllers and multi-FACTS devices in a renewable-integrated deregulated three-area power system.

The overall workflow is summarized in Fig. 1, from the balanced simulation design to the evaluation of controller–FACTS trade-offs. The detailed numerical methodology is described in Section III.

II. THREE-AREA POWER-SYSTEM MODEL AND SIMULATION FRAMEWORK

The simulation framework represents a renewable-integrated three-area power system operating under deregulated electricity-market conditions. The control areas exchange power through tie-lines, and changes in generation or demand produce frequency deviations and departures from scheduled inter-area transfers. Conventional generation, solar and wind resources, EVs and BESSs collectively determine the power balance in each area. AGC coordinates the participating resources to regulate frequency and restore scheduled exchanges following disturbances.

The deregulated operating environment is represented by PoolCo, bilateral and contract-violation scenarios. A DISCO participation matrix (DPM) specifies the allocation of contractual demand among participating generation companies and establishes the corresponding generation obligations and scheduled exchanges [3]. These market conditions influence the corrective power required from each area. Consequently, frequency regulation is evaluated together with deviations from scheduled tie-line

transfers, rather than treating all power exchanges as unscheduled disturbances.

Alternative AGC controllers and FACTS configurations provide the control choices examined in the simulations. Controllers process the area control error (ACE), formed from frequency deviation and net tie-line power deviation, to determine corrective generation commands. FACTS devices modify the network response according to their implemented device models, while EV and BESS participation provides supplementary power support. The resulting dynamic performance depends on the combined operating condition, controller–FACTS configuration and support-resource allocation.

2.1 System configuration

The study system consists of three interconnected control areas (Fig. 2). Each area contains:

• one equivalent generation company (GENCO), represented by a first-order speed governor and a first-order non-reheat turbine;

• one distribution company (DISCO), whose load step is the main disturbance;

• wind and solar generation, represented by step changes in their output, which are the renewable disturbances;

• an aggregated EV fleet and a battery energy storage system (BESS), which provide fast support driven by the local frequency deviation and ACE, at a fixed 5% participation;

• a shunt FACTS channel, active when STATCOM or UPFC is selected, and an AGC controller that acts on the area control error (ACE).

Fig. 2 shows the model as implemented in the simulator.

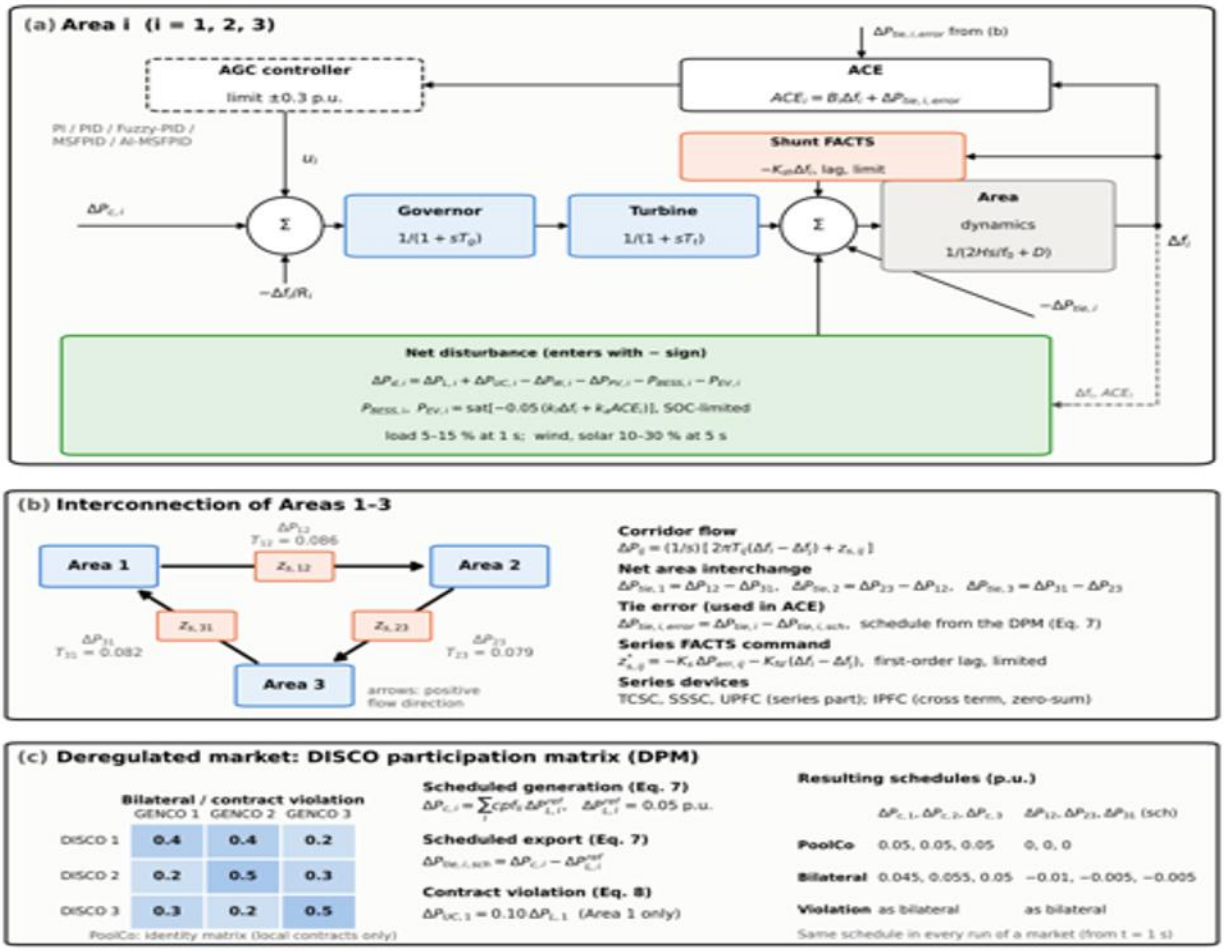


Fig. 2. Three-area system, interconnection and deregulated participation matrix (source project schematic).

Table I. Three-area system and tie-line parameters.

Parameter	Area 1	Area 2	Area 3
Inertia H (s)	5.0	4.5	4.8
Damping D (p.u./Hz)	0.8	0.9	0.85
Droop R (Hz/p.u.)	2.4	2.5	2.45
Governor Tg (s)	0.08	0.09	0.085
Turbine Tt (s)	0.30	0.32	0.31
Frequency bias B (p.u./Hz)	0.425	0.430	0.428
Tie-line T12/T23/T31	0.086	0.079	0.082

2.2 Generation, area and tie-line dynamics

The GENCO of Area i is represented by a speed governor and a non-reheat turbine driven by its scheduled contract generation ΔPc,i and the AGC command ui:

$$\begin{aligned}\frac{d\Delta P_{g,i}}{dt} &= \frac{\Delta P_{c,i}+u_i-\Delta P_{g,i}-\Delta f_i/R_i}{T_{g,i}},\\ \frac{d\Delta P_{t,i}}{dt} &= \frac{\Delta P_{g,i}-\Delta P_{t,i}}{T_{t,i}}\end{aligned} \quad (1)$$

The frequency deviation follows the swing equation with inertia constant Hi and damping Di:

$$\frac{2H_i}{f_0}\frac{d\Delta f_i}{dt} = \Delta P_{t,i} + \Delta P_{sh,i} - \Delta P_{d,i} - D_i\Delta f_i - \Delta P_{tie,i} \quad (2)$$

where ΔPsh,i is the shunt FACTS support and the net area disturbance is

$$\Delta P_{d,i} = \Delta P_{L,i} + \Delta P_{UC,i} - \Delta P_{W,i} - \Delta P_{PV,i} - P_{BESS,i} - P_{EV,i} \quad (3)$$

The incremental power on each tie corridor and the net tie-line power of each area is

$$\begin{aligned}\frac{d\Delta P_{ij}}{dt} &= 2\pi T_{ij}\left(\Delta f_i - \Delta f_j\right) + z_{s,ij},\\ \Delta P_{tie,1} &= \Delta P_{12} - \Delta P_{31},\\ \Delta P_{tie,2} &= \Delta P_{23} - \Delta P_{12},\\ \Delta P_{tie,3} &= \Delta P_{31} - \Delta P_{23}\end{aligned} \quad (4)$$

where zs,ij is the series FACTS output on corridor ij. The area control error is

$$\begin{aligned}ACE_i &= B_i\Delta f_i + \Delta P_{tie,i,error},\\ \Delta P_{tie,i,error} &= \Delta P_{tie,i} - \Delta P_{tie,i,sch}\end{aligned} \quad (5)$$

Governor dead band and generation-rate constraints are implemented in the simulator but were disabled for all runs reported here, so that the comparison isolates the controller, FACTS and market effects; their influence is discussed in Section 5.

2.3 Load, renewable, EV and BESS models

Disturbances. The contracted DISCO load step and the wind and solar fluctuation steps of Area i are

$$\begin{aligned}\Delta P_{L,i} &= \frac{L_i}{100}1(t-1),\\ \Delta P_{W,i} &= \frac{W_i}{100}P_{baseW}1(t-5),\\ \Delta P_{PV,i} &= \frac{S_i}{100}P_{basePV}1(t-5)\end{aligned} \quad (6a)$$

where Li ∈ {5, 10, 15}, Wi ∈ {10, 20, 30} and Si ∈ {10, 20, 30} are the factor levels (%) of the operating pattern, PbaseW = 0.10 p.u. and PbasePV = 0.08 p.u. are the base wind and solar powers of each area, and 1(t − τ) is the unit step applied at t = τ s.

Storage support. The EV fleet and the BESS act as fast supplementary regulators driven by the local frequency deviation and ACE:

$$P_{s,i} = sat\left[-\alpha_s\left(k_{f,s}\Delta f_i + k_{a,s}ACE_i\right)\right], \quad s \in \{BESS, EV\} \quad (6b)$$

where a positive Ps,i denotes injection into the area (Eq. 3). The stored energy Es,i (p.u.h) is updated with the one-way efficiency ηs:

$$\frac{dE_{s,i}}{dt} = \begin{cases}-P_{s,i}/(3600\eta_s), & P_{s,i} \geq 0,\\ -\eta_s P_{s,i}/3600, & P_{s,i} < 0.\end{cases} \quad (6c)$$

with t in seconds and SOCs,i = 100Es,i/Es. Discharge is blocked (Ps,i = 0) when Es,i has reached Es,min, and charging is blocked when Es,i has reached Es,max. The participation is αs = 0.05 in every area and run; kf = 1.0 and ka = 0.2 for the BESS (±0.10 p.u., E = 0.20 p.u.h, initial SOC 60%, limits 20–90%, η = 0.95) and kf = 0.7 and ka = 0.1 for the EV aggregator (±0.08 p.u., E = 0.15 p.u.h, initial SOC 70%, limits 30–90%, η = 0.92). The storage powers and the AGC command are evaluated once per integration step and held constant over the four Runge–Kutta stages.

2.4 Deregulated market representation

Contracts between GENCOs and DISCOs are represented by the DPM [1], whose element cpflk is the fraction of the demand of DISCO l contracted from GENCO k (each DISCO row sums to unity). With one GENCO and one DISCO per area, the scheduled generation of Area i and the scheduled flow on corridor ij (the net bilateral contract between Areas i and j) are computed from the DPM at a reference contracted demand of 0.05 p.u. per DISCO, and are held fixed, from t = 1 s, in every run of a market scenario:

$$\begin{aligned}\Delta P_{c,i} &= \sum_l cpf_{li}\Delta P_{refL,l},\\ \Delta P_{ij,sch} &= cpf_{ji}\Delta P_{refL,j} - cpf_{ij}\Delta P_{refL,i}\end{aligned} \quad (7)$$

The scheduled area exports follow from the corridor schedules in the same way as the actual interchanges in Eq. (4) (ΔPtie,1, sch = ΔP12, sch − ΔP31, sch, and

so on), and equal ΔPc,i − ΔPrefL,i. This gives ΔPc,i = 0.05 p.u. in every area and no scheduled interchange in the PoolCo scenario, and ΔPc,i = 0.045, 0.055 and 0.050 p.u., corridor schedules ΔP12, sch = −0.010, ΔP23, sch = −0.005 and ΔP31, sch = −0.005 p.u. and area exports of −0.005, +0.005 and 0 p.u. in the bilateral and contract-violation scenarios. The scheduled generation covers only the reference demand; because the actual DISCO load step (Eq. 6a) is 0.05, 0.10 or 0.15 p.u., any load above the reference is not covered by the contract schedule and must be supplied through the AGC loop.

In the contract-violation scenario DISCO 1 draws an additional uncontracted load equal to 10% of its load step. It is excluded from the schedule and applied only as a physical load in Area 1 (Eq. 3), so it appears in ACE1 and is taken up by the AGC of Area 1:

$$\Delta P_{UC,1} = 0.10\Delta P_{L,1}, \quad \Delta P_{UC,2} = \Delta P_{UC,3} = 0 \quad (8)$$

The three market scenarios are defined in Table 2. In the PoolCo scenario each DISCO contracts only with the GENCO of its own area, so there is no scheduled interchange; the bilateral scenario uses the cross-area DPM; and the contract-violation scenario uses the bilateral DPM with the uncontracted load of Eq. (8).

Table II. Deregulated market representation.

Market	DISCO participation matrix (rows DISCO 1–3)	Additional load
PoolCo	[1,0,0]; [0,1,0]; [0,0,1]	None
Bilateral	[0.4,0.4,0.2]; [0.2,0.5,0.3]; [0.3,0.2,0.5]	None
Contract violation	Same as bilateral	10% extra DISCO 1 step

2.5 FACTS device models

The FACTS devices are represented at AGC time scale by reduced-order supplementary channels. The model provides a series channel on each tie corridor and a shunt channel in each area; which channels are active depends on the device selected. With the corridor tie error ΔPerr,ij = ΔPij − ΔPij,sch (Eq. 7), the channel commands are

$$\begin{aligned} z^*_{s,ij} &= -K_s\Delta P_{err,ij} - K_{fd}\left(\Delta f_i - \Delta f_j\right), \\ z^*_{sh,i} &= -K_{sh}\Delta f_i \end{aligned} \quad (9a)$$

For the IPFC the series commands of the three corridors are coordinated by a cross-corridor term and a zero-sum projection:

$$\begin{aligned} r_{ij} &= -K_s\Delta P_{err,ij} - K_x c_{ij}, \\ z^*_{s,ij} &= r_{ij} - \tfrac{r_{12}+r_{23}+r_{31}}{3}, \\ c_{12} &= \Delta P_{err,23} - \Delta P_{err,31} \end{aligned} \quad (9b)$$

so that the supplementary power is exchanged internally between the corridors. Each command is limited and passed through a first-order lag, with the same time constant TF for the series and shunt channels:

$$T_F\frac{dz}{dt} = sat(z^*) - z \quad (10)$$

TCSC uses only the series channel (Kfd = 0); SSSC uses the series channel with frequency-difference damping Kfd = 0.0075; STATCOM uses only the shunt channel; UPFC uses the series channel (Kfd = 0) and the shunt channel; and IPFC uses the coordinated series channel of Eq. (9b). The gains, lags and limits are listed in Table 3. In the 'No FACTS' configuration all channels are zero.

Table III. FACTS supplementary-control parameters.

Device	Ks	Kfd/Kx	Ksh	TF (s)	Limit (p.u.)
TCSC	0.08	—	—	0.05	±0.15
SSSC	0.10	Kfd=0.0075	—	0.05	±0.15
STAT COM	—	—	0.08	0.04	±0.15
UPFC	0.14	—	0.08	0.04	±0.20
IPFC	0.16	Kx=0.04	—	0.04	±0.20

2.6 Controller structures

All three areas use the same controller type, each acting on its own ACEi. Every controller output is limited to ±0.3 p.u., with conditional-integration anti-windup (the integrator is frozen while the output is saturated, unless the error drives it back inside the limit) and an integrator clamp at ±0.3/KI. The derivative term uses the filtered ACE derivative ACE′i, computed at each step k as ACE′i,k = ACE′i, k−1 + α [(ACEi,k − ACEi, k−1)/Δt − ACE′i, k−1], with α = NΔt/ (1 + NΔt) and N = 20 rad/s. The PI and PID controllers are

$$u_i = -\left(K_P ACE_i + K_I\int ACE_i\,dt + K_D ACE'_i\right) \quad (11)$$

Fuzzy-PID scales the three gains continuously with z = min (|ACEi|/0.05, 1) and q = min (|ACE′i|/0.1, 1):

$$\begin{aligned} u_i = -[\;& K_P(0.85 + 0.55z + 0.2q)ACE_i \\ &+K_I(1.2 - 0.45z - 0.2q)\int ACE_i\,dt \\ &+K_D(0.75 + 0.3z + 0.65q)ACE'_i] \end{aligned} \quad (12)$$

MSFPID selects one of three gain sets according to the ACE band and adds rate-dependent terms, so that

integral action dominates near steady state and proportional–derivative action dominates large excursions:

$$u_i = -\left(aK_P ACE_i + bK_I \int ACE_i\, dt + dK_D ACE_i'\right), \quad (a,b,d) \in \{(0.9,1.3,0.8),(1.1,1.0,1.05),(1.35,0.7,1.3)\} \tag{13}$$

AI-MSFPID applies bounded multiplicative corrections to the MSFPID gains:

$$u_i = -[\ (1+\gamma_P)aK_P ACE_i + (1+\gamma_I)bK_I \int ACE_i\, dt + (1+\gamma_D)dK_D ACE_i'] \tag{14}$$

The correction is chosen for each operating condition from ten policies (plain MSFPID and nine γ combinations from an L9 array) by a k-nearest-neighbour classifier trained on the lowest-J_dyn safe policy for each of the 81 conditions, falling back to MSFPID when its confidence is below 0.6. In leave-one-out validation it matched the teacher in 48% of conditions; across the 486 AI-MSFPID runs it applied γ = (0, 0.10, 0.05) in 75%, plain MSFPID in 24% and γ = (−0.10, 0.10, 0.10) in 1%.

2.7 Controller gains

The controller gains (Table 4) are fixed design values, identical in all three areas and in all 2,430 runs; they were not re-optimised for individual controllers or operating conditions. The comparison therefore measures the effect of the controller structure at representative fixed gains (read from the Controllers sheet of the input workbook; the gain-retuning option of the simulator was not used), which is the situation of an operator choosing between controller types without re-tuning. The effect of optimising the gains of each structure is discussed in Section 5.

Table IV. Controller gains (identical in Areas 1–3).

Controller	KP	KI	KD	Implementation
PI	0.35	0.18	0	Eq. (11)
PID	0.55	0.30	0.08	Eq. (11)
Fuzzy-PID	0.58	0.32	0.085	Eq. (12)
MSFPID	0.60	0.34	0.09	Eq. (13)
AI-MSFPID	0.60	0.34	0.09	Eq. (14)

2.8 Operating conditions and simulation settings

The operating conditions are defined by the 27 rows of an L27 orthogonal array (Section 3.1, Table 5), each simulated under the three market scenarios, giving 81 operating conditions. Initial deviations are zero, the load steps are applied at t = 1 s and the renewable steps at t = 5 s, and every run is simulated for 100 s with Δt = 0.02 s.

2.9 Performance indices

The settling time is the system settling time: the latest time after which all three area frequency deviations remain within ±0.002 Hz and all three tie-line errors ΔPtie,i,error remain within ±0.002 p.u., taken as the first sample after the last excursion outside either band. All 2,430 runs settled within the horizon (5.76–63.92 s). The integral indices are computed from the summed frequency deviations of the three areas by the trapezoidal rule over 0–100 s:

$$IAE = \int_0^{100} \sum_i |\Delta f_i|\, dt, \quad ISE = \int_0^{100} \sum_i (\Delta f_i)^2\, dt,$$
$$ITAE = \int_0^{100} t \sum_i |\Delta f_i|\, dt,$$
$$ITSE = \int_0^{100} t \sum_i (\Delta f_i)^2\, dt \tag{15}$$

The peak frequency deviation, peak tie-line error and peak ACE are the maxima over time and areas of |Δfi|, |ΔPtie,i,error| and |ACEi|. The composite dynamic index combines error, peak, control-effort and storage-use terms:

$$J_{dyn} = ITAE + 5ISE + 10max|\Delta f| + 5max|\Delta P_{tie,error}| + 0.25\int_0^{100} \sum_i u_i^2\, dt + 0.5(E_{BESS} + E_{EV}) \tag{16}$$

where ITAE and ISE are those of Eq. (15), the peaks are as defined above, and Es = (1/3600) ∫Σi|Ps,i|dt (p.u.h, t in seconds) is the absolute energy throughput of the BESS or EV units of all three areas.

III. METHODOLOGY

The complete simulation and assessment workflow is summarized in Fig. 1. It links the balanced operating design, numerical simulation, dynamic response indices and matched engineering comparisons. The framework is introduced in Fig. 1 and is used to organize the subsequent comparative analysis.

3.1 Simulation Database and Experimental Design

The comparative study uses the final nominal simulation database of 2,430 runs, generated from five AGC controllers, six FACTS configurations, three deregulated market scenarios and 27 three-area operating patterns. For every market and operating pattern, all 30 controller–FACTS pairs are evaluated under the same system model and disturbance settings. This balanced, fully crossed arrangement yields 810 simulations per market, 486 per controller, 405 per FACTS configuration and 81 for each controller–

FACTS cell. Every market–controller–FACTS combination contains 27 operating-pattern observations.

The operating patterns specify area-wise load steps and wind and solar fluctuation steps. Load levels are 5%, 10% and 15% of area rating; wind and solar fluctuations are 10%, 20% and 30% of their respective base renewable powers (0.10 p.u. for wind and 0.08 p.u. for solar). EV and BESS participation remain fixed at 5% in every area and nominal run. The 27 patterns originate from an L27 orthogonal array; although its coded columns are orthogonal, their assignment can alias some renewable effects with load-interaction components. This design feature does not invalidate the balanced, within-pattern controller–FACTS comparisons, but limits independent causal interpretation of all nine disturbance factors.

Factor group	Factors	Levels	Role
Load	Load A1–A3	5, 10, 15%	Area-wise load steps
Wind	Wind A1–A3	10, 20, 30%	Wind fluctuation
Solar	Solar A1–A3	10, 20, 30%	Solar fluctuation
Controller	Controller	PI; PID; Fuzzy-PID; MSFPID; AI-MSFPID	Five strategies
FACTS	FACTS	No FACTS; TCSC; SSSC; STATCOM; UPFC; IPFC	Six configurations
Market	Market	PoolCo; Bilateral; Contract violation	Three scenarios

Table V. Operating factors and levels in the nominal simulation database.

All runs use the system dynamics and fixed controller/device parameters defined in Section II. Load steps occur at 1 s and renewable steps at 5 s; each simulation lasts 100 s with a numerical time step of 0.02 s. Each cell represents a deterministic simulation, not a repeated physical experiment. Consequently, variation across operating patterns should not be presented as measurement noise or independent experimental replication.

The experimental unit is one deterministic response trajectory for a specified combination of operating pattern, market, controller and FACTS configuration. The complete crossing is important: each controller is evaluated under exactly the same 27 disturbance patterns, three market scenarios and six network-support alternatives. Hence, differences between controller marginal means are not caused by unequal representation of load, renewable or contractual conditions. Similarly, each FACTS configuration is evaluated with all five controller structures and all 81 market–pattern cases. The resulting comparisons are conditional on the specified plant and controller gains; they are not independent physical replications.

For reproducibility, the 27-pattern operating matrix should be retained as an immutable case index. A simulation record can be identified by the tuple (pattern, market, controller, FACTS). The disturbance values for Areas 1–3 are obtained from the corresponding row, while the controller and FACTS labels select the parameter sets described in Section II. This indexing prevents accidental comparisons between different disturbance patterns and allows the same scenario to be retrieved for frequency, tie-line and ACE plots.

The three market arrangements represent distinct scheduling conditions. PoolCo uses local contracting and zero scheduled interchange; bilateral trading uses the specified DISCO participation matrix; and contract violation retains the bilateral schedule while introducing additional uncontracted demand in Area 1. The physical disturbance and scheduled interchange must therefore be stored separately. Otherwise, a legitimate scheduled export could be misinterpreted as a regulation error.

The nominal numerical study uses zero initial deviations, a 100 s horizon and a 0.02 s step. Load disturbances begin at 1 s, followed by wind and solar changes at 5 s. The response metrics are calculated using the same time vector for every run. The 27 operating patterns are design points rather than random samples of all possible renewable operating conditions; extrapolation beyond the specified levels is consequently not supported.

3.2 Dynamic Response Evaluation and Comparative Framework

For each simulation, frequency deviations in Areas 1–3, actual-minus-scheduled tie-line errors and area control errors are obtained as time-domain trajectories. Nine smaller-the-better performance responses are

evaluated according to Section 2.9: system settling time, composite dynamic performance index (Jdyn), IAE, ISE, ITAE, ITSE, peak absolute frequency deviation, peak absolute tie-line error and peak absolute ACE.

The evaluation separates recovery behaviour (settling time and time-integrated errors) from transient containment (peak frequency, tie-line and ACE deviations). The composite index additionally includes control effort and storage throughput. This separation is necessary because a controller–FACTS combination may improve the speed of recovery without producing the lowest transient peak, or vice versa.

Response	Mean	SD	Minimum	Maximum
Settling time (s)	22.6886	9.5372	5.76	63.92
Jdyn	8.3566	7.6038	2.07	58.4134
IAE	0.716573	0.379224	0.310628	3.011601
ISE	0.017963	0.013644	0.002369	0.100565
ITAE	7.15968	7.520364	1.223358	56.427535
ITSE	0.069584	0.084403	0.015001	0.776696
Peak Δf (Hz)	0.085711	0.019574	0.026535	0.119892
Peak tie error (p.u.)	0.021708	0.009640	0.000188	0.049235
Peak ACE	0.044700	0.010999	0.011579	0.068926

Table VI. Descriptive statistics for the 2,430 nominal simulations (reported source values).

The settling-time range (5.76–63.92 s) and composite-index range (2.07–58.4134) illustrate variation across the investigated operating conditions and configurations. These ranges are descriptive and do not establish performance beyond the tested design.

Dynamic-response assessment proceeds in two complementary layers. First, the complete trajectories of frequency deviation, actual-minus-scheduled tie-line power error and ACE are examined for representative scenarios. Second, each trajectory is reduced to nine scalar responses using the definitions in Section 2.9. This distinction matters because a single integral index may conceal the timing of a transient, and two responses with similar peak values can exhibit different oscillatory recovery.

The settling-time calculation applies the prescribed bands simultaneously to all three area frequencies and all three-area tie-line errors. For each sampled instant, a Boolean indicator is true only when every monitored signal is within its respective tolerance. The system settling time is the first sample after the final false indicator. This is deliberately more restrictive than quoting the settling time of one area or of frequency alone. The reported range of 5.76–63.92 s refers to this joint definition.

Peak frequency deviation describes the largest absolute frequency excursion, whereas peak tie-line error describes the largest deviation from scheduled exchange. Peak ACE includes both local frequency bias and tie-line regulation error. These measures are related but not interchangeable. In particular, ACE depends on the area bias coefficient, so its magnitude should be compared with external literature only after matching the ACE convention and units.

The four integral measures distinguish amplitude and persistence. IAE weights the absolute error uniformly in time; ISE emphasizes large excursions through squaring; ITAE penalizes errors persisting later in the response; and ITSE combines late-error emphasis with squared amplitude. The composite dynamic index additionally includes control effort and absolute BESS/EV energy throughput. Its fixed numerical weights make it useful for ranking the present simulation cases, but its numerical value should not be treated as a universal physical quality measure.

The archived M03 Case 001 frequency, tie-line and ACE plots are presented as illustrations of the three-area response. Because they depict a single case, they do not establish controller-wide or device-wide superiority. A controlled graphical comparison would hold the operating pattern, market and FACTS choice fixed while varying the controller, or hold the controller fixed while varying the FACTS configuration.

The numerical integration sequence is also important for interpretation. The load and renewable steps are introduced at fixed sample times, and the AGC command and storage support are held constant during

the four stages of each Runge–Kutta update, as stated in Section II. Thus, the controller reacts to the sampled ACE rather than to a continuously updated intermediate-stage control signal. Reproducing the trajectories requires the same order of disturbance update, controller evaluation, saturation, storage-state update and state integration. A different update order could change short-duration peaks even when the nominal differential equations are unchanged.

The performance outputs should be stored together with their units and calculation conventions. Frequency peaks are in hertz, tie-line errors are in per unit, and ACE follows the frequency-bias and interchange-error definition of Section 2.2. The energy-throughput terms in Jdyn are expressed in per-unit hours and use a factor of 1/3600 because simulation time is in seconds. These definitions matter especially when comparing results from different models or plotting data on multiple axes.

It is also necessary to distinguish a system-level maximum from an area-specific response. The reported peak frequency is the largest absolute deviation among all three areas and all-time samples; the peak tie-line error and peak ACE are defined analogously. A figure showing only Area 1 may therefore not reproduce the tabulated system peak. Likewise, the reported system settling time is not simply the largest of three frequency-only settling times because the tie-line tolerances must also be satisfied.

To ensure a fair and consistent evaluation, all five AGC controllers are compared under identical combinations of 27 operating patterns, three deregulated market scenarios, and six FACTS configurations. Similarly, the six FACTS configurations are compared while maintaining the same controller, market scenario, and operating pattern. This matched experimental design minimises the influence of differences in operating conditions and enables a systematic assessment of the relative performance of each controller and FACTS configuration.

For a given performance response, the mean difference between two alternatives, a and b, across N matched operating cases is calculated as

$$\overline{\Delta}_{b-a} = \frac{1}{N}\sum_{i=1}^{N}\left(y_{b,i} - y_{a,i}\right) = \overline{y}_b - \overline{y}_a \quad (17)$$

where y_{ai} and $y_{\beta i}$ represent the performance responses of alternatives a and b under the i-th matched operating condition, respectively. N denotes the number of matched cases, while $\bar{y}_a$ and $\bar{y}_\beta$ represent the corresponding mean response values.

When the reference mean $\bar{y}_a$ is nonzero, the relative mean percentage change is determined using

$$\Delta_{rel}(\%) = \frac{\overline{y}_b - \overline{y}_a}{\overline{y}_a} \times 100 \quad (18)$$

For smaller-the-better performance measures, such as settling time, peak frequency deviation, peak tie-line power error, IAE, ISE, ITAE, ITSE, and the composite dynamic performance index, a negative percentage indicates improved performance of alternative b relative to alternative a, provided the reference mean is positive. Conversely, a positive percentage indicates deterioration.

In the present study, each controller is evaluated across 486 matched operating conditions (27 operating patterns × 3 markets × 6 FACTS configurations). Each FACTS configuration is assessed across 405 matched conditions (27 operating patterns × 3 markets × 5 controllers). Furthermore, every controller–FACTS combination is examined under 81 operating conditions (27 operating patterns × 3 markets).

The statistical assessment considers mean performance values, paired differences, and relative percentage changes to evaluate the effectiveness of the investigated alternatives. Where statistical inference is required, confidence intervals and significance measures should be calculated from the original matched-case simulation results rather than estimated from aggregated descriptive statistics alone.

This approach provides a consistent and reproducible basis for comparing AGC controllers and FACTS configurations while ensuring that observed differences are evaluated under equivalent operating conditions.

Because all controller–FACTS alternatives are evaluated under common scenarios, the results can also be examined separately for PoolCo, bilateral and contract violation. Differences across markets are interpreted in relation to their contractual schedules and uncontracted demand. Any formal significance testing should respect the repeated use of the 27

operating patterns and the deterministic nature of the simulations; nominal run counts must not be mistaken for independent physical replications.

The simulations are deterministic. Therefore, ordinary independent-sample confidence intervals based on 486 or 405 runs would overstate the effective amount of independent disturbance information. If uncertainty intervals are reported, resampling should preserve the common operating-pattern structure, for example by drawing pattern identifiers and carrying all corresponding strategies together. Such intervals characterize sensitivity to the sampled design patterns; they are not estimates of field measurement uncertainty.

Interpretation is based on effect magnitude and response consistency, not merely statistical significance. Controller increments are examined sequentially from PI through PID, Fuzzy-PID, MSFPID and AI-MSFPID. FACTS effects are examined relative to No FACTS, and the market effect is assessed by comparing the three contractual arrangements at matched physical disturbance levels. Where a controller reduces recovery time but not the initial peak, both findings are retained rather than collapsed into a single assertion of superiority.

For an auditable implementation, the matched case identifiers should be sorted before differences are calculated. A controller comparison can be formed by fixing pattern, market and FACTS and subtracting the response for one controller from the response for another. A device comparison fixes pattern, market and controller. Any missing or duplicated identifier should be flagged rather than silently omitted, because imbalance would compromise the paired interpretation. The source study reports a complete 2,430-run nominal dataset.

An effect-size table should retain the baseline value, comparison value, absolute difference and percentage difference. For example, the mean settling-time difference between PI and AI-MSFPID is approximately −17.77 s, while the relative change is −50.0%. Reporting both makes clear that the reduction is not merely a percentage artefact. In contrast, the approximate 4.0% decrease in peak frequency from shunt-capable FACTS is a change of only a few thousandths of a hertz in the reported marginal means.

The use of the 27 operating patterns in all strategy combinations provides a controlled computational comparison but does not create 2,430 independent disturbance realizations. The market and strategy factors are crossed with the same pattern set. Therefore, inference about a wider distribution of operating conditions would require independently sampled patterns or a carefully justified resampling scheme. The present study emphasizes observed matched differences and descriptive distributions rather than treating nominal simulation count as field evidence.

3.4 Engineering Assessment of Controller–FACTS Trade-offs

The final assessment compares each configuration using a response profile rather than relying solely on a single aggregate score. First, controller choices are evaluated for settling time, ITAE and Jdyn. Second, FACTS configurations are examined for peak frequency deviation, peak tie-line error and peak ACE. Third, controller–FACTS pairings are checked for trade-offs between faster recovery and lower peaks under the three market scenarios.

This methodology is deliberately distinct from response-surface fitting and constrained desirability optimization: it assesses the directly simulated dynamic responses under matched conditions. The present data support comparative engineering observations within the investigated design, but do not establish general performance under untested parameter uncertainty, communication attacks or hardware-in-the-loop operation.

Engineering selection is performed as a structured comparison, not as a newly computed global optimization. The first screen compares recovery metrics (system settling time, ITAE and Jdyn); the second compares peak frequency, tie-line and ACE errors; and the third examines whether any gain is consistent across PoolCo, bilateral and contract-violation cases. The controller–FACTS heatmaps summarize 81 market–pattern responses per cell and show whether the best network-support option changes with controller structure.

The interpretation of a configuration depends on the intended objective. A system operator prioritizing frequency containment may prefer the configuration with the smallest peak frequency deviation, while another prioritizing interchange restoration may emphasize tie-line error and settling time. The study does not contain comparable converter costs, losses, maintenance burden or hardware reliability data. Accordingly, economic optimality and field deploy ability cannot be inferred from the dynamic rankings.

A useful non-compensatory screen is to compare the entire response vector of each candidate with that of a reference strategy: a candidate is preferred without a trade-off only when it is no worse on every selected criterion and strictly better on at least one. This is an interpretation rule rather than a claim that a new Pareto set was calculated. Where criteria conflict, the separate differences are presented to preserve the engineering meaning of the trade-off.

IV. RESULTS AND DISCUSSION

4.1 Overview of the nominal simulation evidence

The final V8.8 nominal dataset contains 2,430 deterministic simulations: 27 operating patterns × 3 market scenarios × 5 AGC controllers × 6 FACTS configurations. The balanced crossing gives 486 runs per controller, 405 per FACTS configuration, and 810 per market. All reported averages in this section are taken from the archived V88 nominal summaries; no cyberattack or benchmark-replication runs are mixed into these statistics. The analysis emphasizes direct dynamic performance, rather than repeating the response-surface model adequacy and desirability optimisation of the related RSM study.

Nine smaller-is-better responses characterize recovery and disturbance rejection. The reported settling times span 5.76–63.92 s and the composite dynamic index spans approximately 2.07–58.41. These ranges indicate substantial heterogeneity among operating cases and motivate examining controller and device effects separately rather than selecting configurations solely from a single aggregate index.

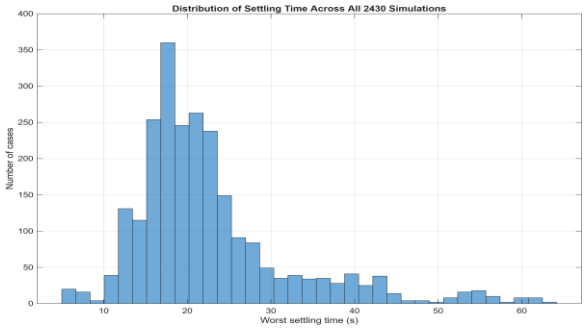


Fig. 3. Distribution of settling time across the 2,430 nominal simulation runs (original V8.8 project export).

The mean settling time of 22.6886 s and standard deviation of 9.5372 s indicate that a single average cannot describe the complete nominal response range. The minimum and maximum settling times, 5.76 s and 63.92 s, reflect substantial differences across the combinations of disturbance pattern and control strategy. The histogram in Fig. 3 makes this variation visible, including the longer-settling tail that would be obscured by a single mean.

The composite index has a mean of 8.3566 and standard deviation of 7.6038, with reported values between approximately 2.07 and 58.41. The spread is comparatively large, consistent with the inclusion of time-weighted error, peak error, control effort and storage throughput in one measure. A low value of this index is desirable under its stated weights, but the separate response metrics remain necessary to identify which aspect of dynamic regulation has improved.

4.2 Controller performance and diminishing incremental gains

Table 7 summarizes the five controller means over identical FACTS, market and operating-pattern combinations. The PI controller has the slowest mean recovery (35.56 s), whereas AI-MSFPID has the shortest (17.79 s). This corresponds to a 50.0% reduction. The composite dynamic index falls from 17.2589 to 5.0707 (70.6% lower), and frequency ITAE from 15.9814 to approximately 3.905, indicating marked reductions in persistent frequency error and composite dynamic penalty. However, mean peak frequency deviation changes much less, from approximately 0.0897 Hz to 0.0840 Hz (6.4%). Thus, faster restoration should not be equated with proportionally smaller initial frequency excursions.

Table VII. Controller-wise nominal performance (N = 486 per controller).

Controller	Settling (s)	Jdyn	Peak Δf (Hz)	Peak tie (pu)	Peak ACE	ITAE
PI	35.5620	17.2589	0.0897	0.0259	0.0480	15.9814
PID	23.0622	8.1955	0.0864	0.0223	0.0453	6.9902
Fuzzy-PID	18.6865	5.9137	0.0843	0.0203	0.0435	4.7455
MSFPID	18.3378	5.3440	0.0841	0.0201	0.0434	4.1762
AI-MSFPID	17.7947	5.0707	0.0840	0.0200	0.0433	3.9051

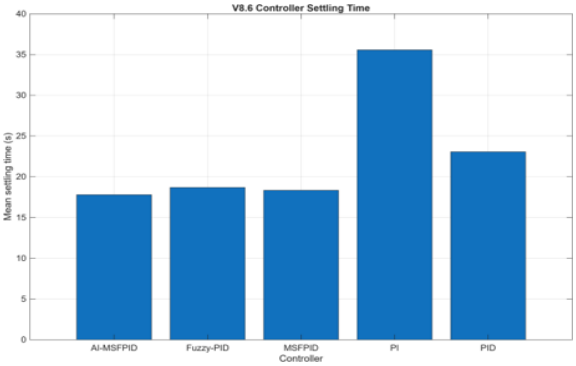


Fig. 4. Mean settling time by AGC controller (V8.8 project export).

The largest performance improvements arise before the most sophisticated controller is reached. Fuzzy-PID settles in approximately 18.69 s, MSFPID in 18.34 s, and AI-MSFPID in 17.79 s. AI-MSFPID therefore improves mean settling time by only about 4.8% relative to Fuzzy-PID and 3.0% relative to MSFPID. This is a meaningful engineering trade-off: the additional supervisory complexity offers comparatively modest mean recovery benefit beyond the established fuzzy and multi-stage alternatives. The source study also reports limited leave-one-out agreement of the AI policy classifier, so these results should not be interpreted as evidence of out-of-sample AI superiority.

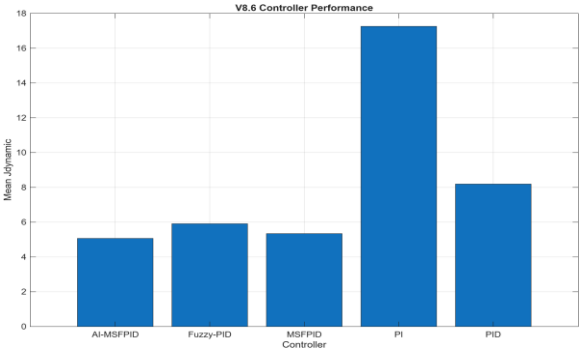


Fig. 5. Controller-wise composite dynamic performance index (V8.8 project export).

The controller comparison exhibits diminishing returns. Relative to PI, PID reduces mean settling time from 35.5620 s to 23.0622 s; Fuzzy-PID reduces it further to 18.6865 s. The remaining reductions to 18.3378 s for MSFPID and 17.7947 s for AI-MSFPID are much smaller. Thus, most of the improvement attributed to the most advanced architecture is already achieved by the transition to fuzzy gain scheduling.

The same ordering is evident in Jdyn: 17.2589 for PI, 8.1955 for PID, 5.9137 for Fuzzy-PID, 5.3440 for MSFPID and 5.0707 for AI-MSFPID. Relative to MSFPID, the AI-assisted correction reduces mean Jdyn by about 5.1% and mean settling time by about 3.0%. This incremental improvement must be weighed against the need to maintain a classifier and validate its policy choices. The reported 48% leave-one-out agreement with the teacher policy limits claims of robust out-of-sample policy identification.

Peak frequency deviation changes much less across the same controller progression: approximately 0.0897 Hz for PI and 0.0840 Hz for AI-MSFPID. The discrepancy between the large reduction in settling time and modest reduction in peak frequency deviation suggests that the controller structure is more influential in the subsequent regulation and recovery than in the earliest excursion caused by the imposed disturbance. This is an interpretation of the tested cases, not a general proof about all AGC systems.

4.3 FACTS-dependent transient performance

The six FACTS conditions each contain 405 runs, allowing comparison at matched controller, market and operating-pattern levels. Table 8 shows that the mean Jdynamic differs relatively little between the No-FACTS, TCSC, SSSC and IPFC conditions. STATCOM and UPFC slightly increase mean settling time and mean Jdynamic in the present reduced-order models, while decreasing mean peak frequency deviation. This is a response-specific trade-off rather than a uniformly superior device outcome.

Table VIII. FACTS-wise nominal performance (N = 405 per configuration).

FACTS	Settling (s)	Jdyn	Peak Δf (Hz)	Peak tie (pu)	Peak ACE
No FACTS	22.6468	8.3258	0.0869	0.0226	0.0455
TCSC	22.5958	8.3097	0.0869	0.0218	0.0454
SSSC	22.5889	8.3073	0.0869	0.0215	0.0453
STATCOM	22.8928	8.4574	0.0834	0.0224	0.0434
UPFC	22.8087	8.4350	0.0834	0.0209	0.0433
IPFC	22.5988	8.3041	0.0869	0.0211	0.0453

Against No FACTS, UPFC changes the mean peak frequency deviation from 0.08687 to 0.08338 Hz (-4.0%), while mean peak tie-line error changes from 0.02259 to 0.02090 p.u. (-7.5%). STATCOM produces a comparable frequency-peak reduction but a smaller tie-line improvement. Series-support options improve tie-line error more than frequency peaks. These comparisons are descriptive averages; they do not include cost, converter losses or switching-level validation.

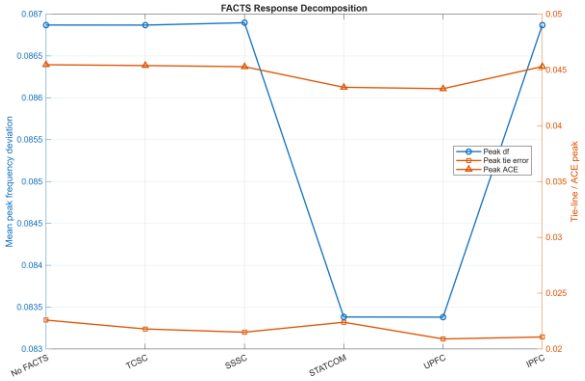


Fig. 6. Response-specific effect of FACTS configurations on nominal dynamic performance (original V8.8 export).

The device means reveal a different pattern from the controller means. The series-oriented TCSC, SSSC and IPFC configurations produce relatively small changes in mean settling time and Jdyn, but reduce peak tie-line error compared with No FACTS. Their benefits therefore appear principally in interchange regulation rather than frequency-peak containment within the reduced-order model.

STATCOM and UPFC, which include shunt support, reduce mean peak frequency deviation from approximately 0.0869 Hz without FACTS to approximately 0.0834 Hz. UPFC additionally lowers mean peak tie-line error to approximately 0.0209 p.u., compared with 0.0226 p.u. without FACTS. Nevertheless, both STATCOM and UPFC have slightly larger mean settling times and Jdyn than No FACTS. These opposing movements demonstrate why the term “best FACTS device” must be qualified by the response objective.

The results are averages across all controllers and market–pattern cases. They do not establish that every individual case benefits from UPFC, nor that a device with a small marginal improvement will retain that improvement when its control parameters or operating conditions change. The controller–FACTS heatmaps should therefore be consulted before selecting a device for a specific controller architecture.

4.4 Influence of market arrangements

PoolCo, bilateral and contract-violation scenarios each contribute 810 runs. Table 9 shows that mean settling time is nearly unchanged across markets, whereas contract violation increases mean peak frequency deviation, tie-line error and ACE. These results are consistent with the additional uncontracted demand imposed in Area 1, which affects the physical disturbance without changing the contractual schedule. Consequently, market effects should be evaluated primarily through peak and interchange metrics rather than mean settling time alone.

Table IX. Market-wise nominal performance (N = 810 per market).

Market	Settling (s)	Jdyn	Peak Δf (Hz)	Peak tie (pu)	Peak ACE
PoolCo	22.6803	8.2658	0.0836	0.0210	0.0434
Bilateral	22.6822	8.2808	0.0845	0.0216	0.0446
Contract violation	22.7035	8.5231	0.0890	0.0225	0.0461

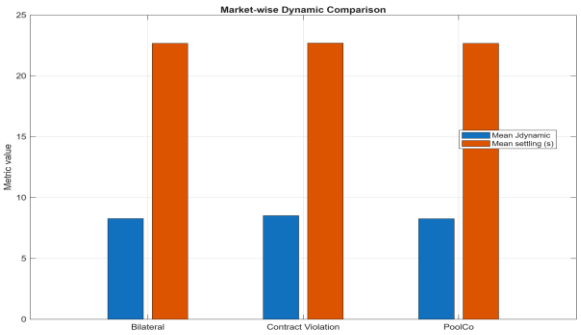


Fig. 7. Comparison of nominal dynamic responses across deregulated market scenarios (V8.8 project export).

The mean settling times under PoolCo, bilateral and contract violation are approximately 22.6803, 22.6822 and 22.7035 s, respectively. Their proximity indicates that the contractual arrangement has little effect on this particular aggregate recovery measure in the nominal model. This should not be interpreted as identical dynamic behaviour, because the markets have different scheduled interchanges and, in the violation case, different physical demand.

Mean peak frequency deviation increases from approximately 0.0836 Hz under PoolCo to 0.0845 Hz under bilateral trading and 0.0890 Hz under contract violation. Peak tie-line error similarly increases from about 0.0210 to 0.0216 and 0.0225 p.u.; peak ACE increases from 0.0434 to 0.0446 and 0.0461. These changes are consistent with the additional Area 1 uncontracted load, which the AGC must correct without a corresponding revision of scheduled interchange.

This distinction is relevant to deregulated operation: recovery time alone can miss the increased transient regulation burden imposed by contract violations. Evaluating scheduled tie-line error and ACE alongside frequency deviation provides a more complete assessment of the market-related disturbance.

4.5 Controller–FACTS interaction and practical selection

The 30-cell controller–FACTS summary contains 81 matched operating/market cases per combination. The heatmaps provide a useful complement to controller-only and FACTS-only means: they show whether the response to a network-support configuration changes with controller architecture. A device should therefore be screened against a specified controller and response objective, not selected solely from its grand mean. The heatmaps below summarize the archived Jdynamic and settling-time cell averages; they do not represent independent uncertainty estimates.

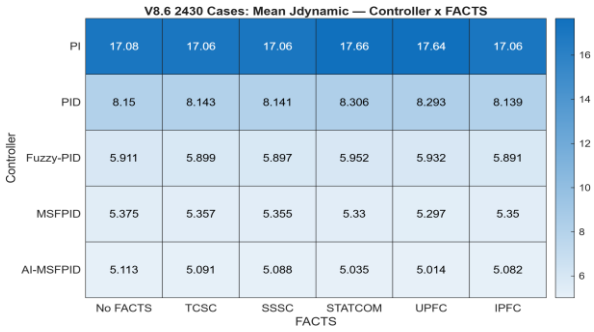


Fig. 8. Controller–FACTS cell means for the composite dynamic index (81 cases per cell).

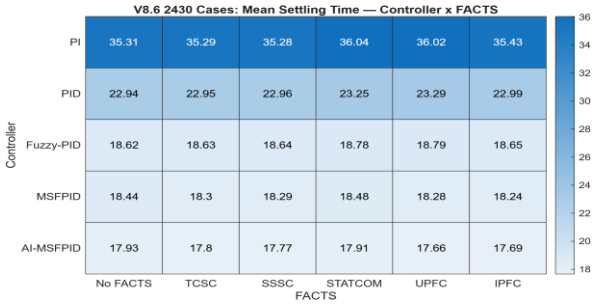


Fig. 9. Controller–FACTS cell means for settling time (81 cases per cell).

4.5.1 Illustrative three-area time-domain responses

The following original project plots illustrate the time-domain outputs of the three-area simulator for archived Module M03, Case 001. They are a single-case diagnostic illustration, not matched controller–FACTS overlays or evidence of an average effect. They complement, but do not replace, the aggregate controller and FACTS comparisons reported above.

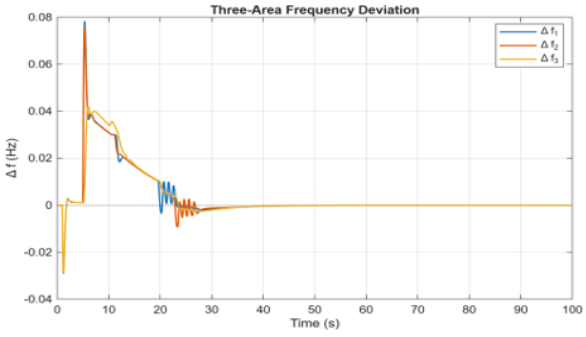


Fig. 10. Frequency deviations Δf of Areas 1–3, archived M03 Case 001. The common trajectory plot illustrates inter-area frequency coupling and transient restoration.

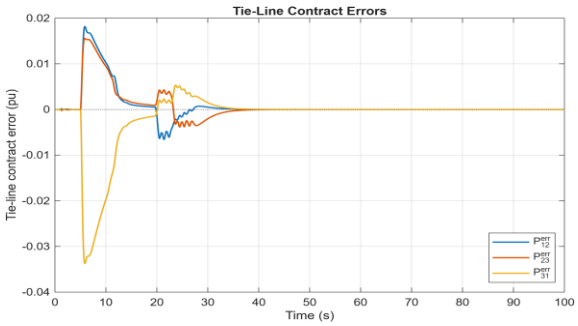


Fig. 11. Actual-minus-scheduled tie-line power error, archived M03 Case 001. The figure illustrates why scheduled interchange must be separated from physical flow.

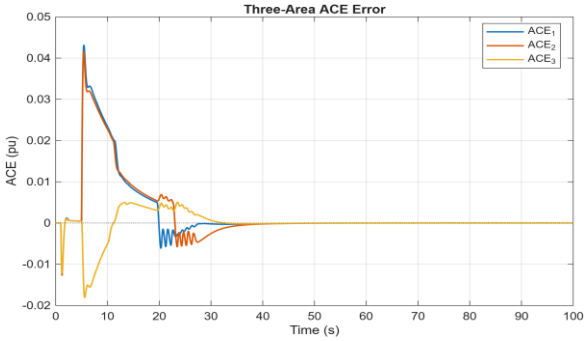


Fig. 12. Area control error trajectories for Areas 1–3, archived M03 Case 001. ACE combines local frequency bias and scheduled tie-line error.

The two controller–FACTS heatmaps provide a compact visual summary of the crossed design. Each cell averages 81 matched market–operating cases, so rows can be compared at common FACTS conditions and columns at common controller conditions. The strong row-wise separation in Jdyn and settling time indicates that controller structure is the principal source of the large recovery differences shown in the plots. Differences among columns are smaller and should be interpreted relative to the response metric under consideration.

The archived three-area time-domain plots show the qualitative sequence of a disturbance response: an initial deviation after the imposed step, oscillatory interaction among areas, and eventual restoration toward the reference condition. The tie-line plot uses actual-minus-scheduled interchange, which is essential under bilateral transactions. The ACE plot reflects both frequency bias and interchange deviation. These figures establish the physical meaning of the measured quantities, but a single example cannot substitute for matched overlays across all controller choices.

For future graphical validation, a representative operating pattern should be selected in advance, with the same market, disturbance values and FACTS device used for all five controllers. A complementary device comparison should fix AI-MSFPID and vary only the six FACTS configurations. Such overlays would test whether the improvements visible in aggregate tables correspond to more rapid damping and smaller excursions in directly comparable trajectories.

Controller–FACTS interactions should be interpreted in terms of whether the relative device ordering changes across controller rows. A small spread among FACTS columns for PI does not necessarily imply the same spread for AI-MSFPID. Conversely, an apparent difference between two cells may be too small to justify additional device complexity. The heatmaps are useful for screening such patterns, but their displayed cell means do not provide device cost, sensitivity to model uncertainty or stability margins.

From an engineering perspective, the choice between MSFPID and AI-MSFPID is especially relevant. The advanced policy improves the reported mean recovery and composite index only incrementally over the multi-stage baseline, while adding classification and policy-selection logic. This does not negate the observed benefit, but it changes the decision question: the additional algorithm should be justified by performance consistency, reliability and implementation burden, not solely by superiority over PI.

The results also separate two forms of support. A controller changes the corrective generation command generated from ACE, while a FACTS configuration modifies the modeled network-support channels. Their different locations in the regulation loop help explain why large reductions in recovery metrics can coexist with relatively small changes in peak frequency, and why a series-support device can improve tie-line error without appreciably changing the frequency peak. This explanation remains specific to the reduced-order model and selected device gains.

4.6 Engineering interpretation and practical implications

Three conclusions follow directly from the nominal data. First, controller architecture has a strong

association with recovery speed and accumulated frequency error under the fixed-gain comparison. Second, FACTS configurations provide smaller but metric-specific benefits, particularly in peak frequency and tie-line error. Third, contractual violations increase peak regulation burdens even when mean settling time changes little. These statements concern the tested parameterization and should not be generalized to untested controller retuning, nonlinear constraints, hardware implementations or cyberattack conditions.

4.7 Comparison with previous studies

The results are consistent with the broader literature showing that improved AGC controller structures can reduce recovery time and accumulated frequency error. Panda and Yegireddy [6] examined multi-objective tuning of conventional controllers, whereas the present work compares five fixed-gain controller architectures on a balanced common operating design. Thus, the reported 50.0% settling-time reduction from PI to AI-MSFPID should be interpreted as a within-model comparison, not as a direct numerical improvement over the different plants and tuning methods used in earlier studies.

Dash et al. [3] compared several FACTS devices with optimised two-degree-of-freedom controllers, and Pilla et al. [4] investigated FACTS-assisted fuzzy-PID regulation. Their studies support the relevance of supplementary network control, but direct percentage comparisons are not justified without identical plant parameters, disturbance magnitudes, device models and performance definitions. In the present simulations, STATCOM and UPFC reduce mean peak frequency deviation by approximately 4.0% relative to No FACTS, whereas UPFC reduces mean peak tie-line error by approximately 7.5%. These are response-specific effects, not proof that UPFC is universally optimal.

Studies involving EVs and storage, including Lalngaihawma et al. [5] and Tasnin and Saikia [7], investigate resource participation as an active design choice. By contrast, EV and BESS participation are fixed at 5% in this nominal dataset; their comparative contribution cannot be inferred from the controller and FACTS marginal means. Similarly, the present results do not demonstrate the hardware or field performance of the controller structures. The literature comparison is therefore qualitative and scoped to the methodological differences.

Table X. Methodological comparison with representative published AGC investigations.

Study	Main emphasis	Difference from present assessment
Panda & Yegireddy [6]	Multi-objective PI/PID tuning	Five fixed-gain controller structures compared across common conditions
Dash et al. [3]	Optimised 2DOF control with multiple FACTS	Six network-support configurations crossed with five controllers
Pilla et al. [4]	FACTS-assisted fuzzy PID	Device effects compared across alternative controller structures
Lalngaihawma et al. [5]	Renewables and EVs in deregulated AGC	EV/BESS held fixed; focus on controller and FACTS response
Present study	2,430 nominal simulations; three markets	Matched recovery, frequency, tie-line and ACE assessment

The comparison with earlier work is methodological rather than a numerical benchmark ranking. Panda and Yegireddy [6] emphasize multi-objective controller tuning; the present study holds the specified gains fixed while changing controller structure. Dash et al. [3] and Pilla et al. [4] investigate FACTS-assisted AGC with different controller and plant assumptions. Lalngaihawma et al. [5] and Tasnin and Saikia [7] address renewable, EV or storage participation, whereas those support levels are fixed in the nominal database analyzed here.

Consequently, the percentage reductions reported in this paper should not be directly compared with percentages from those publications without matching the plant model, system base, disturbance sizes, controller tuning procedure, settling tolerance and measurement horizon. The present contribution is the transparent within-model comparison of recovery and peak-control trade-offs over a balanced controller–FACTS–market design.

4.8 Limitations and further validation

The present conclusions are restricted to the deterministic V8.8 nominal simulation design: 27 operating patterns, three deregulated markets, five controllers and six FACTS configurations. Controller gains are fixed, EV and BESS participation is fixed at 5% in each area, and the FACTS devices use reduced-order AGC-scale models. These conditions permit balanced comparisons but do not establish general performance under independent operating patterns, parameter uncertainty, communications disturbances, hardware constraints or different tuning budgets.

Further work should evaluate matched time-domain overlays of Δf, scheduled tie-line error and ACE for the same disturbance and market condition; assess independent controller retuning; and validate representative controller–FACTS pairs under nonlinear governor constraints, realistic renewable trajectories and hardware-in-the-loop tests. The related RSM manuscript uses the same simulation platform and dataset; its statistical model-adequacy and desirability-optimisation findings are not claimed as new contributions here. Editorial disclosure and an independent scientific contribution remain necessary before separate submission.

The present analysis has three boundaries. First, the nominal disturbances are step changes, whereas real renewable fluctuations are often time varying and correlated across areas. Second, governor deadband and generation-rate limits were disabled in the reported runs, and therefore the results do not quantify their effect on recovery or actuator demand. Third, the FACTS devices are represented by supplementary AGC-scale channels rather than detailed converter switching models. These modeling choices make the balanced comparison tractable but constrain the physical conclusions.

Numerical verification should include step-size sensitivity for representative cases, consistency checks on the scheduled interchange sign convention, and reconciliation of calculated scalar indices with the saved trajectories. Validation against a published benchmark should reproduce that benchmark's own system parameters and settling definitions before comparing performance. Such work would strengthen confidence in the numerical implementation without altering the scope of the present descriptive comparisons.

Future research can extend the design by varying EV and BESS participation, introducing realistic renewable time series, incorporating governor nonlinearities and communication disturbances, and retuning each controller under a common optimization budget. These are separate questions from the fixed-gain nominal comparison presented here. Their results should not be inferred from the current 2,430-run summaries.

V. CONCLUSIONS

Across the 2,430-run balanced nominal design, the controller structure has a strong effect on settling time and accumulated regulation error. Relative to PI, AI-MSFPID reduces mean settling time by 50.0% and the composite dynamic index by 70.6%; however, most of the gain is already obtained by Fuzzy-PID and MSFPID. FACTS effects are more targeted: STATCOM and UPFC reduce mean peak frequency deviation by approximately 4%, and UPFC reduces mean peak tie-line error by approximately 7.5%. Contract violation increases peak regulation demands while having little effect on average settling time. These findings apply to the documented fixed-gain deterministic simulation design. Independent numerical-convergence checks, matched time-domain overlays, and further validation are needed before extrapolation to field operation.

REFERENCES

[1] V. Donde, M. A. Pai, and I. A. Hiskens, "Simulation and optimization in an AGC system after deregulation," *IEEE Transactions on Power Systems*, vol. 16, no. 3, pp. 481–489, 2001, doi: 10.1109/59.932285.

[2] Demiroren and H. L. Zeynelgil, "GA application to optimization of AGC in three-area power system after deregulation," *International Journal of Electrical Power & Energy Systems*, vol. 29, no. 3, pp. 230–240, 2007.

[3] P. Dash, L. C. Saikia, and N. Sinha, "Comparison of performances of several FACTS devices using cuckoo search algorithm optimized 2DOF controllers in multi-area AGC," *International Journal of Electrical Power & Energy Systems*, vol. 65, pp. 316–324, 2015, doi: 10.1016/j.ijepes.2014.10.015.

[4] R. Pilla, A. T. Azar, and T. S. Gorripotu, "Impact of flexible AC transmission system devices on automatic generation control with a metaheuristic based fuzzy PID controller," *Energies*, vol. 12, no. 21, Art. no. 4193, 2019, doi: 10.3390/en12214193.

[5] S. Lalngaihawma *et al*., "Automatic generation control of hybrid sources incorporating renewable energy sources and electric vehicles in an interconnected power system considering a deregulated environment," *IEEE Access*, vol. 12, pp. 124764–124789, 2024, doi: 10.1109/ACCESS.2024.3454229.

[6] S. Panda and N. K. Yegireddy, "Automatic generation control of multi-area power system using multi-objective non-dominated sorting genetic algorithm-II," *International Journal of Electrical Power & Energy Systems*, vol. 53, pp. 54–63, 2013, doi: 10.1016/j.ijepes.2013.04.003.

[7] W. Tasnin and L. C. Saikia, "Performance comparison of several energy storage devices in deregulated AGC of a multi-area system incorporating geothermal power plant," *IET Renewable Power Generation*, vol. 12, no. 7, pp. 761–772, 2018, doi: 10.1049/iet-rpg.2017.0582.